MANCHESTER 1824
The University of Manchester

The University of Manchester Research

Probabilistic Assessment of the Effect of a Spatially Distributed Hybrid Renewable Energy Source Plant on System Transient Stability

DOI:
10.1109/PMAPS53380.2022.9810614

Document Version
Accepted author manuscript

Link to publication record in Manchester Research Explorer

Citation for published version (APA):
Radovanovic, A., Huang, H., & Milanovic, J. V. (2022). *Probabilistic Assessment of the Effect of a Spatially Distributed Hybrid Renewable Energy Source Plant on System Transient Stability*. Paper presented at 17th International Conference on Probabilistic Methods Applied to Power Systems (PMAPS 2022), Manchester, United Kingdom. https://doi.org/10.1109/PMAPS53380.2022.9810614

Citing this paper
Please note that where the full-text provided on Manchester Research Explorer is the Author Accepted Manuscript or Proof version this may differ from the final Published version. If citing, it is advised that you check and use the publisher's definitive version.

General rights
Copyright and moral rights for the publications made accessible in the Research Explorer are retained by the authors and/or other copyright owners and it is a condition of accessing publications that users recognise and abide by the legal requirements associated with these rights.

Takedown policy
If you believe that this document breaches copyright please refer to the University of Manchester's Takedown Procedures [http://man.ac.uk/04Y6Bo] or contact uml.scholarlycommunications@manchester.ac.uk providing relevant details, so we can investigate your claim.

OPEN ACCESS

Download date:21. Oct. 2022

This is accepted version of the paper published in PMAPS 2022

Probabilistic Assessment of the Effect of a Spatially Distributed Hybrid Renewable Energy Source Plant on System Transient Stability

Ana Radovanović, Student Member *IEEE*
Department of Electrical and Electronic Engineering
The University of Manchester
Manchester, UK
ana.radovanovic@manchester.ac.uk

Haowen Huang
Department of Electrical and Electronic Engineering
The University of Manchester
Manchester, UK
haowen.huang-3@postgrad.manchester.ac.uk

Jovica V. Milanović, Fellow *IEEE*
Department of Electrical and Electronic Engineering
The University of Manchester
Manchester, UK
milanovic@manchester.ac.uk

***Abstract*— Due to the interest in both the environmentally sustainable development and the flexibility of power system, hybrid renewable energy source (HRES) plant has become an attractive research topic. HRES plant represents a mix of various generation and storage technologies seen as a single entity from the perspective of system operators. This paper investigates the impact of a spatially widely distributed HRES plant on transient stability of transmission network on the basis of three representative 24-hour operation scenarios. Probabilistic approach is used for performing transient system stability analysis. The transient stability index is chosen for assessing the influence of the HRES plant on transient system stability. The study is carried out on a large 255-bus transmission system containing four realistic transmission networks. The simulations are conducted in Matlab and DIgSILENT/PowerFactory software environment.**

Keywords*— *hybrid renewable energy source plant, probabilistic modelling, transient stability

I. INTRODUCTION

Over the years, there has been a growing interest in renewable energy sources (RESs) due to the progressive depletion of traditional fossil fuels and the overall environmental degradation. RESs, such as wind and solar energy, are being integrated into power systems all over the world. For instance, the installation capacity of RES power plants in the United Kingdom increased from 8 GW in 2009 to about 50 GW at the end of 2020 [1]. However, the variability and non-dispatchability of these sources makes the use of an RES technology as a single energy source in a power plant unreliable from the perspective of power supply [2]. Consequently, hybrid renewable energy source (HRES) plant has received considerable attention due to its potential to mitigate the stochasticity of individual RESs while preserving the environment.

HRES plant refers to any power plant consisting of more than one type of energy technologies (generation, storage) [3]. Multiple technologies have a single point of interconnection and the whole HRES plant is seen as a single resource from the perspective of the operator [4]. The idea of HRES plant concept is to aggregate different technologies to obtain stable and controllable power production as in the case of conventional power plants. As a result, HRES plants can participate in energy markets and provide ancillary services traditionally obtained from synchronous generators (SGs). In addition, HRES plant structure can be more easily adapted to meet new market requirements compared to single RES technology-based plant and this flexibility in plant configuration is of particular interest to investors. The most common projects involve combinations of battery energy storage systems and photovoltaic (PV) plants and/or wind farms (WFs) [4]. The use of hydro power plants in HRES plants is receiving a significant attention as well [4]. A combination of 29 MW solar plant and 50 MW WF was installed in India in 2018 [5]. HRES plant consisting of a 194 MW WF and a 20 MW battery energy storage system was put in operation in Australia in 2020. In the United States, three plants combining PV and biomass generation sources with the total capacity of 19 MW are in operation [6]. At the end of 2020, 226 HRES plants were installed in the United States with the total of 29.4 GW generation and 0.8 GW storage capacity [6]. It is expected that a significant number of large grid –connected HRES plants will be integrated into power systems in the future [7].

Research on HRES plants has been mainly devoted to the optimal location, design and economic dispatch of HRES plants [8]. On the other hand, the impact of HRES plants on system dynamic behaviour has been commonly neglected in studies. In case of a large number of traditional single RES technology-based plants and HRES plants in power systems as well as decommissioned conventional generators, optimal economic commitment of generation units may result in power system instability. Under such conditions in power system, it may be necessary to take into consideration system dynamic constraints when deciding on the optimal dispatch of individual plants within the HRES plant as well as the optimal dispatch of SGs in the rest of the system for a certain time interval.

This paper investigates the influence of a spatially widely distributed HRES plant on transient stability of a large interconnected transmission network. This is a departure from conventional approach of defining HRES plant as a group of different RES technologies connected to the same point of common coupling. Instead, the paper considers that one owner, e.g., independent generation or RES generation aggregator, may have several RES power plants of the same or different technologies spread across the network and that they may provide their services of stable and controllable power production to transmission system operator, though it may not be delivered at the same "point of entry" in the network. The considered HRES plant consists of wind and solar technologies. The study is performed using three representative system operating scenarios in a large, 255-bus,

978-1-6654-1211-7/22/$31.00 ©2022 IEEE

interconnected transmission system comprising four individual realistic transmission networks with 42 equivalent SGs. Each operating scenario involves a 24-hour transient system stability assessment in a probabilistic manner (probabilistic modelling of power outputs of individual RES technologies within the HRES plant and probabilistic representation of the global transient system stability results). Transient stability index (TSI) is used for describing the overall transient system stability status. The correlation between the distribution of RES power production across the test transmission system (that is, HRES plant spatial composition) and the transient system stability performance is analyzed. All simulations were carried out in a mixed Matlab and DIgSILENT/PowerFactory environment.

II. Methodology

The methodology for assessing the influence of the distributed HRES plant on the transient stability of the system relies on the probabilistic modelling of power outputs of RESs and probabilistic representation of the transient stability results (i.e., TSI values). Adequate probability distribution functions (PDFs) are used for random sampling of production of individual RES power plants within the HRES plant for the considered system operating points. The most probable TSI for the particular operating condition is determined according to the PDF obtained on the basis of TSI values for a large number of system disturbances, and then used for assessing the impact of the HRES plant spatial composition on the overall transient stability performance of the system. The flow chart of the methodology is shown in Fig. 1. The procedure comprises three parts. Part I and Part III, which are mainly focused on data analysis, are performed in Matlab R2020a [9], while Part II (system stability analysis) is run in DIgSILENT/PowerFactory 2020 environment [10].

Firstly, a test scenario (TS) corresponding to a 24-hour transient system stability assessment is chosen from a pre-defined set of TSs (block {1} in Fig. 1). Each TS is associated with a particular daily system loading profile (block {2} in Fig. 1). For each hour in the chosen TS, the power outputs of RES plants within the HRES plants are defined in a probabilistic manner (block {3} in Fig. 1) by sampling the RES power output from the predefined probabilistic distributions. In the case of WFs, it is assumed that the wind speed follows a Weibull distribution with a shape parameter of 2.2 and scale parameter of 11.1 [11]. The power production for the sampled wind speed is obtained from a typical wind turbine power curve [12]. When it comes to PV plants, the production levels are generated assuming that the sun irradiation follows a Beta distribution [13] with the following parameters: a=13.7 and b=1.3 [14].

Pre-disturbance power outputs of SGs in the network are obtained from the results of the optimal power flow (OPF) performed in Part II of the methodology (block {5} in Fig. 1). In order to take into consideration the reduction in the total system inertia level due to HRES plant integration, it is assumed that each SG in the test network is an equivalent generator of a power plant having the maximum four identical units in operation. For a specific plant power output (obtained from the OPF calculation), the maximum number of units in the plant that can be disconnected is determined according to the minimum required operating capacity of the plant (1) [15]:

$$MVA_{SG_i,Min}=\frac{P_{SG_i}}{(1-SCap_{SG_i})\cdot Npf_{SG_i}}, \quad (1)$$

where $MVA_{SG_i,Min}$ is the minimum required operating capacity of the plant for a given plant production, P_{SGi} is the dispatch of the i-th SG in MW, $SCap_{SGi}$ is the spare reserve of the i-th SG in p.u. and Npf_{SGi} is the rated power factor of the i-th SG. A fixed spare capacity of 15% and a rated power factor of 0.85 are adopted [15].

The OPF is performed in DIgSILENT/PowerFactory environment using the detailed system model. The interior point method (the algorithm for AC OPF in DIgSILENT/PowerFactory) is used for solving the optimization problem. The OPF is conducted twice. In the first OPF, all SGs in the test system are in service and have the maximum rated capacity (i.e., it is assumed that all four units in the plant are in service). The results of the first OPF, which depend on the actual output of RESs in the system, are then used to identify which SGs should be disconnected (if calculated generator output is below the minimum allowed power level, the generator is disconnected from the system). The second OPF recalculates the power outputs of SGs after disconnecting certain generators according to the results of the first OPF. In both OPF calculations, the objective is to minimize the total generation cost while satisfying the specified total system load and considering the constraints in terms of real and reactive power outputs of SGs, bus voltage magnitude, line and transformer loadings.

Following the OPF, the pre-disturbance operating condition of the whole network is identified. The next step involves performing system stability simulations in DIgSILENT/PowerFactory software. Transient system stability is assessed through electromechanical simulations (block {6} in Fig. 1). Three-phase self-clearing short-circuit faults at the middle of all transmission lines are considered as representative system disturbances for transient stability assessment. The adopted fault duration is 100 ms. Only three-phase faults are considered as they usually result in the most severe system conditions. For each transient system stability simulation, TSI value is calculated according to the following expression (2) (block {8} in Fig. 1):

$$TSI=100\cdot\frac{360-\delta_{max}}{360+\delta_{max}}, \quad (2)$$

where δ_{max} represents the maximum rotor angle deviation between any two SGs in the network at the same moment after a disturbance. Negative TSI values indicate transient system instability.

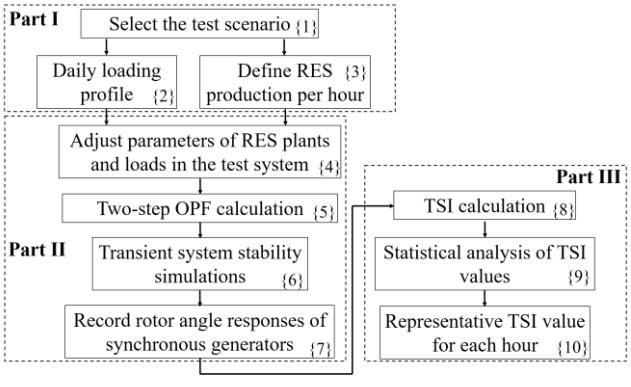

Fig. 1. The flow chart of the methodology.

Part III involves statistical analysis of the obtained TSI values. Given that a large number of three-phase short-circuit faults are simulated per hour in the TS, the most probable TSI value is defined for each hour, and then used as a representative TSI value for the given hour in the further analysis. For each hour in the TS, the non-parametric Kernel PDF is estimated on the basis of the relevant TSI values (block {9} in Fig. 1) [16]:

$$\hat{f}_h(\mathrm{x})=\frac{1}{nh}\sum_{i=1}^{n} K\left(\frac{x-x_i}{h}\right), \quad (3)$$

where $\hat{f}_h(\mathrm{x})$ is the Kernel density estimation of the unknown PDF *f*, *x* is a random variable, *n* is the number of samples in the dataset, *K* is the non-negative Kernel function with the integral equal to one, and *h* is the bandwidth.

The normal distribution with zero mean and standard variance of one is used as a Kernel function as it is the most widely applied [16]. When it comes to the bandwidth, the optimal value of the parameter *h* is defined using the solve-the-equation plug-in method as it has shown the best performance among many other bandwidth estimation techniques [17]. TSI value corresponding to the maximum value of the estimated PDF is selected as the representative TSI value for the analysed operating point/hour in the TS (block {10} in Fig. 1).

III. Test System

A. Modelling of the Test Network

The test system is a simplified, realistic representation of a 255-bus equivalent of four interconnected real transmission networks in Europe comprising 42 SGs and 178 loads. The network structure, as shown in Fig. 2, is divided into four areas connected by 17 tie-lines (TLs). Due to confidentiality reasons, the detailed single line diagram of the network cannot be shown in the paper. The HRES plant in the test system consists of RESs (WFs and PV plants) that are spatially widely distributed in four areas. RES plants are marked in Fig. 2 as "*RESx*", where *x* is a number from 1 to 21 and from 1 to 32 in the case of the Current and Future RES state, respectively (a detailed explanation of the Current and Future RES state is provided in the following Section III B).

The test system is developed in DIgSILENT/PowerFactory software environment. The standard sixth- and fifth-order SG model is used for modelling thermal and hydro power plants, respectively. The control systems of SGs include excitation systems and governors. Given that the focus of the analysis is on electromechanical oscillations (with frequency between 0.2 Hz and 2 Hz), it is assumed that the whole drive system is made up of a single mass, and thus can be represented by a single inertia [18]. The inertia of the SG model includes the inertia of the turbine and generator rotor. Wind turbines and PV units are represented by Double Fed Induction Generators (DFIGs) and Full Converter Connected (FCC) units, respectively. RES power plants contain a number of identical units connected in parallel. The rated power output of individual units in WFs and PV plants is 2 MW. It is assumed that units in service operate at the rated power output, so the number of units in operation is defined by the total power production of the RES power plant. PV plants do not have reactive power capability, while a wind generator produces 0.25 Mvar. The structures of dynamic controllers of WFs and PV plants are in line with guidelines given in [19-21] and suitable for large system stability studies. Detailed description of the dynamic models of RES power plants can be found in [15]. System loads are modelled using a constant power load model.

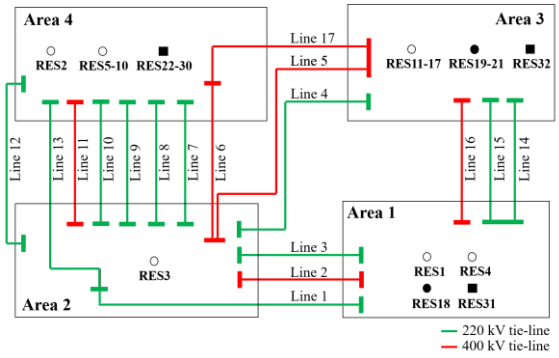

Fig. 2. The schematic diagram of the test system (circles indicate RES plants in the Current RES state; dot and square symbols indicate RES plants installed in the Future RES state).

B. Test Scenarios

Three TSs involving different loading and RES states are defined to reflect realistic system operation and shown in Table I. The maximum and minimum loading corresponds to a system operating condition in winter and summer of 2017, respectively [22], and the corresponding system loading curves are illustrated in Fig. 3. Both RES states from Table I are designed according to the values reported by the respective transmission system operators and their more detailed description is given in Table II. RES state at present, i.e., the Current RES state in Table I and Table II, includes 17 WFs (no PV plants among the installed RESs). The total installed WF capacity at present is 1190 MW (Area 1: 168 MW, Area 2: 86 MW, Area 3: 374 MW, Area 4: 562 MW), which is 9.4% of the installed SG capacity. Considering future network development, the installation capacity of the existing WFs will increase, WFs at new locations will be installed, and there will be further PV plants connected to the system. Therefore, the Future RES state, as referred to in this paper, will include 21 WFs and 11 PV plants, with the total installed capacity of 7908 MW (62.4% of the installed SG capacity). The WF installation capacity in the Future RES state per area is: Area 1: 1112 MW, Area 2: 86 MW, Area 3: 5192 MW, Area 4: 1048 MW. When it comes to PV plants, nine out of eleven PV plants are to be installed in Area 4 with the total capacity of 300 MW, while Area 1 and Area 3 are going to contain a 100 MW and a 70 MW PV plant. RES plants included in the Current RES state are marked by circles in Fig. 2, while WFs and PV plants planned to be installed in the future are represented by black dots and squares in Fig. 2, respectively.

TABLE I. Test Scenarios

Scenario Number	Loading level	RES state
TS 1	Maximum loading	Current RES
TS 2	Maximum loading	Future RES
TS 3	Minimum loading	Future RES

RES penetration level at each hour of the TS is defined as follows:

$$RES_{Level,i}(\%)=\frac{P_{HRES_i}}{P_{Load_i}}\cdot 100, \quad (4)$$

where P_{HRES_i} and P_{Load_i} is the total HRES plant production and the total system load at the i-th hour, respectively. RES penetration levels at each hour of the analysed TSs are shown in Fig. 4. As can be seen, the average RES penetration levels for the three test TSs are about 10%, 30%, and 60%, respectively.

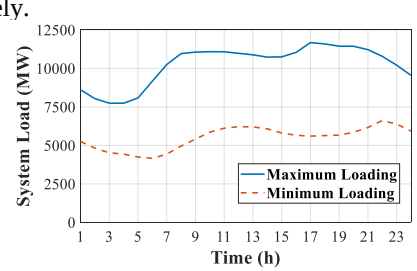

Fig. 3. Maximum (blue solid) and minimum (orange dashed) system loading curves.

TABLE II. RES STATES

RES state	Number of WFs	Total WF capacity	Number of PV plants	Total PV capacity
Current	17	1190 MW	0	0 MW
Future	21	7438 MW	11	470 MW

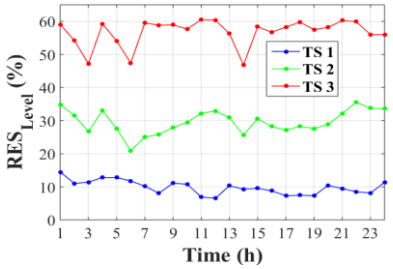

Fig. 4. RES penetration levels for each hour in TS 1 (blue), TS 2 (green) and TS 3 (red).

IV. RESULTS AND DISCUSSION

As described in Section II, 24 hour-transient system stability assessment is performed for each of the three TSs. The Kernel PDF is estimated using the simulated TSIs and the most probable TSI value is defined for each hour in the TSs. In the case of TS 1, the PDF of the obtained TSI values for each hour can be represented by the Weibull distribution as well. The values of the scale parameter are between 68 and 74 for all hours. The shape parameter of the Weibull distributions is within the range [70-120] for hours 01:00 – 07:00 and 24:00, while it is about 58 for the remaining hours during the day. None of the standard, well-known PDFs can be used for representing the PDF of TSIs for most of the hours during the day in TS 2 (TSI values for few hours follow the Weibull or normal distribution) as well as any hour in TS 3, and the Kernel distribution is the only PDF that provides satisfactory results for these operating conditions.

In order to simplify the representation of the results, TSI values presented in Fig. 5 are the most probable TSI values (according to the estimated Kernel PDFs) for each hour in the TSs. Fig. 5 shows the change of TSI during the day for three TSs in order to show the overall transient system behaviour. According to Fig. 5, the TSI calculated under TS 1and TS 2 always keeps a high value during the day (over 70 most of the time), while TSI exhibits greater variations in TS 3 with the largest drop in TSI value observed at hours 4:00, 19:00 and 21:00 (at these hours RES energy injected into the system from Area 3 is at least seven times larger than RES production in Area 1 and RES13 in Area 3 has the largest power output).

In TS 1 the change in TSI over a day follows, to a great extent, the trend of system daily loading profile. The number of SGs in service is higher in this scenario than in TS 2 and TS 3 due to higher loading and lower RES penetration level, which in turn provides very stable transient behaviour of the system during the whole day. By comparing TSI in TS 1 and TS 2 in Fig. 5, where the system loading is the same but RES penetration is different, it can be observed that TSI values in TS 2 (the Future RES state) have a higher magnitude during the low load periods of the day. This suggests that the HRES plant with larger installed capacity could contribute to system transient stability during the periods of low system demand as more of the SGs in the system would operate with higher spare capacity. This though is not a straightforward conclusion to make as the future locations, not only installed capacity, of individual generation technologies within the HRES plant, may be different from the ones in the existing RES state and hence result in different generation dispatch and different power flows in the system. The consistency in improved TSI values during the low load period though suggests that the available RES capacity (and consequential de-loading of SGs) might have the dominant effect.

Focusing on TS 2 and TS 3, where the integrated RES capacity is the same (the Future RES state) but the loading level is different, it can be seen that the TSI value in TS 2 (the Maximum loading) is generally higher (system is more stable) than in TS 3 (the Minimum loading). System operation at the minimum loading level implies that the participation of SGs is small. Lower number of traditional generators in service results in the lower total system inertia level, which results in the deterioration of transient system stability performance. Further inspection of TS 3 revealed that the high values of TSI in TS 3 (70 and above) are related to SG23 in Area 3. In the case of these operating conditions (hours 10, 11, 13, 15, 17, 18, 20, 22 and 24), the committed capacity of SG23 is larger than 410 MVA (i.e., three or four units in the plant are in operation). The only exception is hour 18:00 characterized by SG23 out of service, but associated with the highest system inertia level among all hours during the day (the total system inertia constant at 18:00 h is 4 seconds compared to the value of about 3 seconds for the remaining hours during the day).

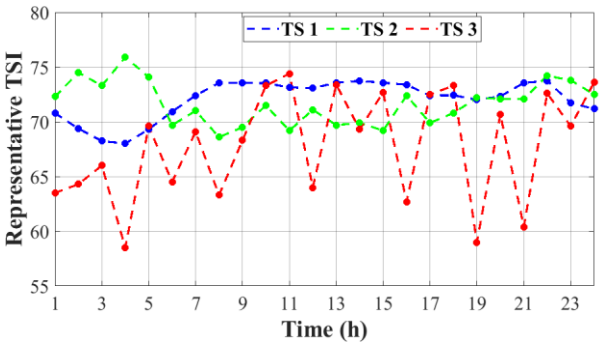

Fig. 5. Representative TSI values for each hour in the TSs.

In order to further analyze the impact of economic dispatch of generation units on transient system stability performance, in each TS additional analysis is carried out for hours with similar total HRES plant production and total system demand to investigate the correlation between RES power distribution across the network (i.e., HRES plant spatial

composition) and the most probable TSI value for the considered operating condition. Similarity in HRES plant production and system load is necessary in order to decouple the impact of HRES plant power output and HRES plant spatial composition on TSI. The share of RES production in Area 2 in the total HRES plant power output is significantly smaller compared to the other three areas in both RES states and thus not taken into account in this analysis.

In the case of TS 1, there are four groups of operating points characterized by similar total HRES plant power output and system demand and they are given in Table III (*Note*: In Table III - V, "*Share_x*" represents the participation of RES production in Area *x* in the total HRES plant power output, while the TSI values correspond to the most probable TSI values for the chosen hours). As seen in Table III, the most probable TSI values for hours within the same group are almost identical. In the case of Groups 1 and 2, the maximum difference between the shares of individual areas' RES production in the total HRES plant output for the operating conditions in the group is below 5%. As for the remaining two groups, larger differences between HRES plant spatial compositions for the hours in the same group can be observed. For instance, the amount of RES power produced in Area 3 is around 5 times larger than in Area 1 at 22:00 h (Group 3), while this ratio is equal to 1.7 at 15:00 h (Group 3). Similarly, RES power output in Area 3 and Area 4 is about 3 and 5, respectively, times larger than RES production in Area 1 for the operating point at 18:00 h (Group 4), while similar amount of RES power is produced in Areas 1 and 3 at 17:00 h (Group 4) and is equal to a half of RES production in Area 4 at the same hour. Given that RES penetration level (calculated according to Eq. (4)) is around 10% for the selected hours from TS 1, change in RES power distribution across the system has almost no effect on the optimal economic dispatch of SGs. The average difference between SG power outputs for the hours within the same group is less than 2.5 MW.

TABLE III. SELECTED OPERATING POINTS FROM TS 1

Group	Hour	TSI	P_{HRES} (MW)	P_{Load} (MW)	Share_1 (%)	Share_3 (%)	Share_4 (%)
1	9:00	73.5	976	8776	8.4	34	53
	10:00	73.5	948	8797	12.9	32	55
2	11:00	73.1	610	8792	19	37	42
	12:00	73.1	570	8712	19.7	32	39
3	14:00	73.7	792	8518	13.6	33	44
	15:00	73.6	814	8530	16.5	29	53
	22:00	73.7	832	8556	7.9	37	43
4	17:00	72.4	676	9266	21.9	24	41
	18:00	72.4	686	9197	9.6	27	51

Three groups of two hours with similar HRES plant power production and system load level are identified in TS 2 (see Table IV). Similar to TS 1, operating conditions within the group result in similar transient system stability performance (the maximum difference between the most probable TSI values for the hours in the same group is 2) regardless of RES power distribution across the test system. The participation of individual areas in the HRES plant production is similar for the pair of hours in Group 1. When it comes to Groups 2 and 3, the main difference is in RES power distribution across Areas 1 and 3. Namely, in the case of operating point at 11:00 h (17:00 h) from Group 2 (3) similar amount of RES power is produced in Areas 1 and 3, while RES power in Area 1 corresponds to about 20% of RES power in Area 3 at 12:00 h (18:00 h) from the same group. Unlike in TS 1, the number and rated capacity of SGs in operation is not the same for operating points in the same group. However, the differences are not significant and do not influence the overall system dynamic performance.

TABLE IV. SELECTED OPERATING POINTS FROM TS 2

Group	Hour	TSI	P_{HRES} (MW)	P_{Load} (MW)	Share_1 (%)	Share_3 (%)	Share_4 (%)
1	9:00	71	2448	8776	10	60	25
	16:00	72.7	2472	8759	15	69	15
2	11:00	69	2832	8792	34	40	23
	12:00	71	2868	8712	11	50	36
3	17:00	69.5	2516	9266	32	47	19
	18:00	70.5	2598	9197	14	60	23

Finally, three groups with three time samples can be used for analyzing the influence of HRES plant composition on the global transient system stability status in TS 3 and are given in Table V. Hours from Group 1 (10:00, 15:00, and 20:00) result in similar TSI. On the other hand, the most probable TSI values for operating conditions from other two groups depend on HRES plant spatial composition. Different RES shares of Areas 1 and 3 for the hours within the same group represent a major cause of their different transient system stability statuses. Namely, operating points with similar HRES plant power output and system demand result in similar TSI values if differences between their RES shares of Area 1 and Area 3 are about 10% (operating points from Group 1, 12:00 h and 21:00 h from Group 2, 16:00 h and 19:00 h from Group 3). RES power provided by Area 1 and Area 3 is very similar at 11:00 h (Group 2) and 17:00 h (Group 3), while RES production in Area 3 is at least 4.5 times larger than in Area 1 in the case of other operating points from Groups 2 and 3. Hours 11:00 and 17:00 are associated with higher TSI value (74.4 and 72.5 for 11:00 h and 17:00 h, respectively) compared to other hours within their respective groups (TSI value for these operating conditions is about 60).

TABLE V. SELECTED OPERATING POINTS FROM TS 3

Group	Hour	TSI	P_{HRES} (MW)	P_{Load} (MW)	Share_1 (%)	Share_3 (%)	Share_4 (%)
1	10:00	73.3	2594	4496	31	49	20
	15:00	72.7	2608	4469	26	46	27
	20:00	70.7	2620	4504	26	56	18
2	11:00	74.4	2832	4684	34	40	23
	12:00	63.4	2868	4750	11	50	36
	21:00	60.4	2858	4745	7	63	28
3	16:00	62.7	2472	4359	15	69	15
	17:00	72.5	2516	4319	32	47	19
	19:00	59	2508	4363	9	68	19

HRES plant spatial compositions for characteristic hours (i.e., a pair of hours characterized by different representative TSI values) from Groups 2 and 3 are illustrated in Fig. 6 (a) and Fig. 6 (b), respectively, using dots of different colours and sizes. The sizes of the dots in Fig. 6 reflect the RES share of individual areas in the total HRES plant production. Furthermore, RES power plant with the highest power production (RES1) is located in Area 1 at 11:00 h and 17:00 h, whereas the highest individual RES power plant output comes from Area 3 in the case of the remaining hours from Groups 2 and 3 (the relevant plants are RES11, RES13, RES14 and RES15, all of them located in a geographically small region). When it comes to the operating points from Group 1, RES power plant with the highest generation is in Area 1 for hours 10:00 and 20:00 (RES18 and RES1,

respectively, which are geographically close to each other), while it is located in Area 4 at 15:00 h. However, the second largest RES power plant output at 15:00 h is produced in Area 1 (RES18), and the difference between the top two RES power plant outputs for this hour is only 38 MW.

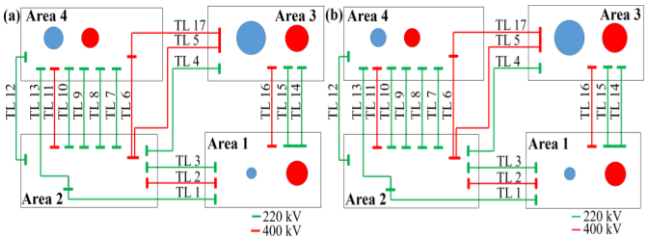

Fig. 6. Illustration of HRES plant spatial composition for characteristic hours from TS 3: (a): Group 2: hour 11:00 (red) and hour 21:00 (blue); (b): Group 3: hour 17:00 (red) and hour 19:00 (blue).

The previous analysis demonstrated that: i) the configuration of SGs in service at hours characterized by similar TSI values is very similar, if not identical; ii) the difference between SG economic dispatches for hours with different TSI values is considerably larger. Therefore, it can be concluded that the location and number of SGs in operation, influenced by the location and output of RESs (i.e., HRES plant spatial composition) and total system demand, affect the transient stability of the power system with a high RES penetration level.

V. Conclusion

This paper presented the investigation of the impact of the geographically distributed HRES plant on transient stability of a large interconnected transmission network. Three representative operation scenarios involving different combinations of loading and RES states are simulated over a 24-hour time period. Though, at the first site the analysis performed may look very similar to conventional study of the effect of large penetration of RESs on system performance, there is one marked difference which is the assumption of coordinated deployment of RESs across the system. The coordinated deployment aims to maximise the offset of generation from SGs (to reduce cost and environmental effects) while deploying the optimal composition of individual RES technologies within the HRES plant (geographically spread across the system) to insure desired system stability performance.

It is demonstrated that both, the system loading level and the HRES plant spatial configuration affect the system stability. Larger system loading, hence smaller relative participation of RESs, generally has a positive impact on transient system stability, while the future RES configuration could lead to either better or worse transient stability. The spatial configuration of HRES does not influence system transient stability in the case of low RES penetration levels (below 30% in analysed cases), however, in the case of higher penetration level of about 60% this influence becomes much more prominent. The location and output of individual RESs in the HRES plant affect the location and number of SGs in operation, and consequently their rotor angle responses to system disturbances. Therefore, the deployment of individual RES plants within spatially distributed HRES plant, in cases of higher penetration levels of RESs in the system, should be decided after assessing overall system transient (and other) stability performance. The conventional economic dispatch in these cases may lead to inadequate system dynamic performance.

Acknowledgment and Disclaimer

This research is supported by the EU H2020 project CROSSBOW (Grant Agreement no. 773430). This paper reflects only the author's views and neither the Agency nor the Commission are responsible for any use that may be made of the information contained therein.

References

[1] Energy trends: September 2021. [Online]. Available: https://assets.publishing.service.gov.uk/government/uploads/system/uploads/attachment_data/file/1021915/Energy_Trends_September_2021.pdf.

[2] F. Blaabjerg, Y. Yang, D. Yang, and X. Wang, "Distributed power-generation systems and protection," Proceedings of the IEEE vol. 105, no. 7, pp. 1311 - 1331, July 2017.

[3] M. K. Deshmukh, and S. S. Deshmukh, "Modeling of hybrid renewable energy systems," Renew. Sust. Energ. Rev., vol. 12, no. 1, pp. 235-249, January 2008.

[4] M. Ahlstrom, et al., "Hybrid resources: challenges, implications, opportunities, and innovation," IEEE Power and Energy Magazine, vol. 19, no. 6, pp. 37 - 44, November-December 2021.

[5] Siemens Gamesa Renewable Energy. [Online]. Available: https://www.siemensgamesa.com/products-and-services/hybrid-and-storage.

[6] R. Wiser, et al., Hybrid power plants: status of installed and proposed projects. Lawrence Berkeley National Laboratory, Berkeley, CA 2020.

[7] W. Gorman, et al., "Motivations and options for deploying hybrid generator-plus-battery projects within the bulk power system," Electr. J., vol. 33, no. 5, pp. 1-15, June 2020.

[8] A. Hina Fathima, and K. Palanisamy, "Optimization in microgrids with hybrid energy systems - a review," Renew. Sustain. Energy Rev., vol. 45, pp. 431-446, May 2015.

[9] MATLAB and Statistics Toolbox Release 2020a. The Mathworks, Inc., Natick, Massachusetts, United States.

[10] "DIgSILENT PowerFactory 2020 User Manual," DIgSILENT GmbH, 2020. [Online]. Available:https://www.digsilent.de/en/powerfactory-download.html.

[11] R. Preece, and J .V. Milanović, "Tuning of a damping controller for multiterminal VSC-HVDC grids using the probabilistic collocation method," IEEE Trans. Power Del., vol. 29, no. 1, pp. 318–326, February 2014.

[12] Vestas Americas Inc., "V80-2.0 MW: Unsurpassed reliability and performance at high-wind sites in North America," 2011. [Online]. Available: http://www.vestas.com

[13] M. Fan, V. Vittal, G. T. Heydt, and R. Ayyanar, "Probabilistic power flow studies for transmission systems with photovoltaic generation using cumulants," IEEE Trans. Power Syst., vol. 27, no. 4, pp. 2251–2261, November 2012.

[14] S. Tao, Y. Ruoying, Z. Lingzhi, and G. Shan, "Power system probabilistic production simulation containing large-scale wind power and photovoltaic power," in Proc. IEEE PES Asia-Pacific Power Energy Eng. Conf, 2013, pp. 1-6.

[15] P. N. Papadopoulos, and J. V. Milanović, "Probabilistic framework for transient stability assessment of power systems with high penetration of renewable generation," IEEE Trans. Power Syst., vol. 32, no. 4, pp. 3078-3088, July 2017.

[16] J. Han, M. Kamber, and J. Pei, Data mining concepts and techniques, 3rd ed., Waltam, USA: Elsevier Inc., 2012.

[17] M. C. Jones, J. S. Marron, and S. J. Sheather, "A brief survey of bandwidth selection for density estimation," J. Amer. Statist. Assoc., vol. 91, no. 433, pp. 401-407, March 1996.

[18] P. Kundur, Power system stability and control, New York, USA: McGraw-Hill, 1994.

[19] Wind turbines – Part 27 – 1: Electrical simulation models – Wind turbines, 2015.

[20] WECC Wind Power Plant Dynamic Modeling Guide, WECC Renewable Energy Modeling task Force, Salt Lake City, UT, USA, January 2014.

[21] WECC PV Power Plant Dynamic Modeling Guide, WECC Renewable Energy Modeling task Force, Salt Lake City, UT, USA ,May 2014.

[22] ENTSO-E Transparency Platform. [Online]. Available: https://transparency.entsoe.eu.